Final Draft

of the original manuscript

Zeng, Z.; Cong, B.; Oliveira, J.; Ke, W.; Schell, N.; Peng, B.; Qi, Z.; Ge, F.; Zhang, W.; Ao, S.:

Wire and arc additive manufacturing of a Ni-rich NiTi shape memory alloy: Microstructure and mechanical properties.

In: Additive Manufacturing. Vol. 32 (2020) 101051.

First published online by Elsevier: 10.01.2020

https://dx.doi.org/10.1016/j.addma.2020.101051

Wire and arc additive manufacturing of a Ni-rich NiTi shape memory alloy: microstructure and mechanical properties

Z. Zeng[1], B.Q Cong[2], J.P. Oliveira[3], B. Peng[1], Z.W. Qi[2], F.G Ge[1], W. Zhang[4], S.S. Ao[4*]

1. *School of Mechanical and Electrical Engineering, University of Electronic Science and Technology of China, Sichuan 611731, China*
2. *School of Mechanical Engineering and Automation, Beihang University, Beijing 100191, China*
3. *UNIDEMI, Department of Mechanical and Industrial Engineering, NOVA School of Science and Technology, NOVA University Lisbon, 2829-516 Caparica, Portugal*
4. *School of Material Science and Engineering, Tianjin University, Tianjin 300072, China*

* Corresponding author: S.S. Ao, E-mail: ao33@tju.edu.cn
Telephone: +86 022 8535 6663; Address: School of Material Science and Engineering, Tianjin University, Tianjin 300072, China

Abstract: Wire and Arc Additive Manufacturing (WAAM) was used for fabrication of NiTi parts using a dedicated Ni-rich NiTi wire as the feedstock material. The as-built parts are fully austenitic at room temperature as confirmed by differential scanning calorimetry, X-ray diffraction and superelastic cycling. The as-built microstructure changed from collumnar, in the first deposited layers, to equiaxed in the last deposited ones as a result of the different thermal cycle conditions. This is the first work where WAAM NiTi parts exhibit superelastic behavior under tensile conditions, highlighting the potential use of the technique for the creation of complex shaped parts based on this material and process.

Keywords: NiTi shape memory alloy, WAAM, Phase transformation, Microstructure, Digital image correlation

1. Introduction

NiTi shape memory alloys (SMAs) are used in multiple industries (e.g. automotive,

aerospace, robotic, and biomedical), as a result of their shape memory and superelastic properties [1]. Both properties occur due to a thermodynamic and crystallographic reversible martensitic transformation [2]. Although NiTi SMA research has taken place for nearly six decades now, and has been implemented in several applications, SMAs applications are still limited to simple geometries processed by laser [3-5], Tungsten Inert Gas (TIG) [6], electrical resistance [7] or ultrasounds [8].

With the advent of additive manufacturing, complex shaped parts which could not be obtained by conventional manufacturing routes are now possible [9]. The majority of SMAs research work conducted to date has focused on powder-bed systems using a laser [10,11] or an electron beam [12-14] as the heat source. The application of multiple additive manufacturing techniques to create NiTi parts have been extensively described by Elahinia et al. [15, 16].

NiTi parts created by selective laser melting (SLM) can exhibit superelastic properties in the as-built condition [17] or after appropriate post-process heat treatments [18,19] which incorporate compression techniques A multi-scale shape memory effect in SLM NiTi parts was also observed by Hamilton et al. [20] and this can be attributed to a gradient of microstructures along the as-built part due to the thermal cycle imposed during production [21]. Additionally, owing to the typically fast thermal cycles during SLM, nanoscale precipitates such as Ni_4Ti_3 can be formed [22].

Some of the shortfalls of laser and electron beam powder-based additive manufacturing techniques include the high costs of equipment and powder feedstock, as well as slow production rates. Despite these limitations, these processes are still extremely common due to no other fusion-based additive manufacturing technique being capable of replicating the precision and accuracy of these processes at this time. Another critical issue often found during SLM of NiTi parts is the lack of evaluation of the part's mechanical properties under tensile conditions. Such can be attributed to the high probability of defects, such as lack of fusion or porosity, that may occur in powder-bed systems.

Wire and arc additive manufacturing (WAAM), which is an alternative additive manufacturing technique, is capable of achieving high production rates at the expense

of geometrical tolerance. Here, a wire acts as the feedstock material while an arc-based heat source promotes its deposition onto a substrate. As a result, three dimensional parts can be created by the deposition of multiple layers similar to SLM. The use of WAAM for the creation of metallic parts is often associated with a low number of defects, provided that the process parameters are optimized [23]. As a result, parts created by WAAM can be evaluated under compression [24] but also under tension conditions [25, 26], which further expands the potential application of this technique for more demanding applications. The potential of WAAM to create large complex-shaped parts with short delivery times has attracted the attention of the aerospace industry in this technology. In fact, WAAM has been already successfully applied to the fabrication of different metallic components, such as aluminum [27-30], titanium [31, 32] and steel [33].

A preliminary investigation into the use of WAAM to create NiTi parts was recently presented by Wang et al. [34]. The authors were able to create walls using Ni and Ti wires, fed separately? into the weld pool. The as-built parts were mechanically characterized, and the fracture strain ranged between 4.1 and 5.5%. No evaluation of the superelastic response was performed, which is fundamental to understand the feasibility of the WAAM technique to preserve this important functional property. It is also noted the NiTi walls were created with a tandem-like system using two feedstock wires. This option is technically more challenging than using only one feedstock wire and may pose potential problems to control the composition of the as-built material, which for NiTi shape memory alloys must be very precise [35].

Since there is commercially available NiTi wire, it is possible to use it as the feedstock material. This solution has the advantage of using the exact composition desired for the as-built parts, since most of NiTi wires available can be selected in advance. Therefore, if desired, is it possible to select Ti-rich NiTi wire for parts to be martensitic at room temperature, or Ni-rich NiTi to be austenitic at room temperature.
In this work, a commercially available Ni-rich NiTi wire was used to create walls with WAAM technology. The microstructural evolution along the as-built part was studied by means of microscopy techniques, differential scanning calorimetry and X-ray

diffraction. Additionally, the mechanical properties were evaluated using tensile testing until fracture, and superelastic cycling. This is the first work on WAAM of NiTi SMAs reporting the existence of superelastic behavior in the as-built parts under tensile testing conditions. These results open the door for WAAM to provide a new means of producing complex shaped NiTi shape memory alloys.

2. Materials and experiments

In this investigation, 0.7 mm diameter Ni-rich (50.5 at.%) NiTi wire was deposited onto a NiTi baseplate using a conventional TIG torch as the WAAM heat source. The setup is depicted in Fig.1. A direct current (75A) combined with an ultra-high frenquency pulse (current: 50A, frequency: 20kHz, duty cycle: 50%) was selected as the current mode of the arc. A local Ar (99.99% pure) shielding device was used to minimize oxidization. To create thin walls, the travel speed of the torch, wire feed speed, and the Ar flow rate were set at 0.2 m/min, 0.9m/min, and 15L/min respectively.

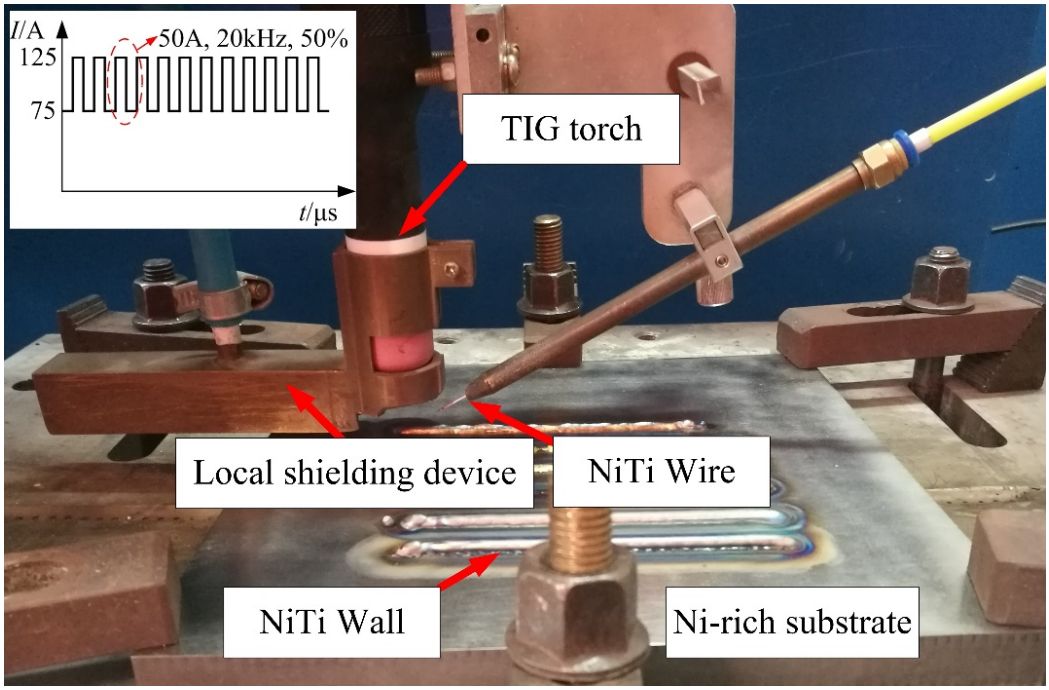

Figure 1 Experimental setup of the WAAM process

Metallographic specimens were cut vertically to the deposited height. For microstructural observation, these specimens were prepared using conventional

metallographic techniques. Then, the WAAM specimens were etched using a H_2O:HNO_3:HF solution for 5 to 10 seconds. The as-built microstructure was examined using an Olympus optical microscope, a JSM-6490LV scanning electron microscope (SEM) equipped with an energy dispersive spectroscopy (EDS) system, and X-ray diffraction (XRD). Vickers micro-hardness measurements along the sample height was performed with a series of 100 g indents, held for 15 seconds.

The transformation temperatures were characterized by Differential Scanning Calorimetry (DSC) following the ASTM F2004-05 standard. The heating/cooling rate was set at 5°C/min. The transformation temperatures were determined as described in the literature (DOI: 10.1088/0964-1726/25/8/085001).

Parts for tensile testing were obtained by wire cutting from the deposited layers along the horizontal direction (X-Y in Fig.2a) with 40mm length and 1mm thickness, shown in Fig.2b. An Instron 5548 micro-tensile tester was used to assess the as-built mechanical properties of three samples at a strain rate of 0.4%/s. Digital image correlation (DIC) was used during the tensile tests with a resolution of 4000 x 3000 pixels and a focal length of 50 mm, to evaluate local changes in the mechanical properties of the parts. The fracture surfaces after tensile testing were analyzed by SEM. The superelastic behavior under tensile conditions was evaluated by loading up to 6% strain and then unloading to a zero-stress condition. 10 load/unload cycles were imposed to the as-built WAAM NiTi parts. The accumulated irrecoverable strain after each cycle was determined [36].

3. Results and Discussion

3.1 Microstructure, hardness and chemical composition

Fig.2a depicts the top bead appearance of the as-deposited NiTi parts. It can be seen that the deposited beads are uniform throughout the deposition without evidence of discontinuities. Additionally, the as-built wall is characterized by a bright silver color, which indicates that no evidence of surface oxidation is present. This is of special importance for NiTi, due to high susceptibility to oxidation at elevated temperatures, which is known to degrade the mechanical and functional properties of the material

[37].

Fig.2c depicts the X-Z cross-section view of 5 deposited layers. Each layer was marked using dashed red lines. Equiaxed grains are visible on the Ni-rich substrate and these will support the formation of columnar crystals in the first deposited layer.

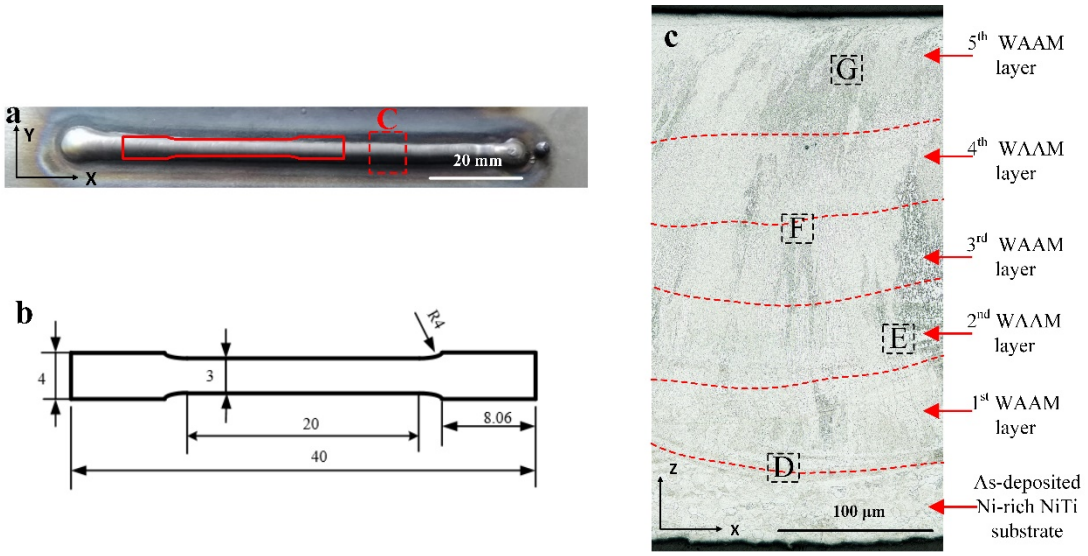

Figure 2 a) Macroscopic appearance of the WAAM NiTi specimens; b) Mechanical testing samples dimensions (mm) c) Microstructure of the as-buit part

The high cooling rate of the first deposited layer is enhanced by the cold and large substrate which rapidly dissipates heat, further influencing a columnar-like microstructure to form in this region, highlighted in Fig.3a. It can be observed that the columnar grains in the first deposited layer present an inclination in the growth direction towards the center of the fusion zone. These elongated grains occur as a result of the heat source movement and of the large local heat flux from the center of the fusion zone pool to the end of the weld pool tail (DOI:10.1063/1.5098371). With subsequent depositions, the thermal gradient is reduced due to the intrinsically low thermal conductivity of this class of alloys and lower cooling rates of the deposited material due previous depositions, which creates a pre-heating effect. As a result, the columnar grain inclination is limited as additional WAAM deposits are made. Partial remelting of the already solidified grain occurs on the following deposition. Then, the existing equiaxed grains at the top of the fusion zone grow by epitaxy, contrary to the direction of heat

extraction. As a result, needle-like grains are formed, and these are observed at the interface of subsequent deposited layers shown in Fig.3b.

For the following depositions, the cooling rate decreases since the already deposited layers promote a pre-heating effect. As a consequence, the as-solidified microstructures change to an equiaxed morphology (see Fig.3c). Additionally, compared with the microstructure in the first deposited layers, a noteworthy decrease in the grain size occurs in the last deposited layer. The microstructural differences in terms of grain morphology occur due to the different thermal cycle conditions experienced, namely the decrease of the cooling rate with consecutive depositions of material.

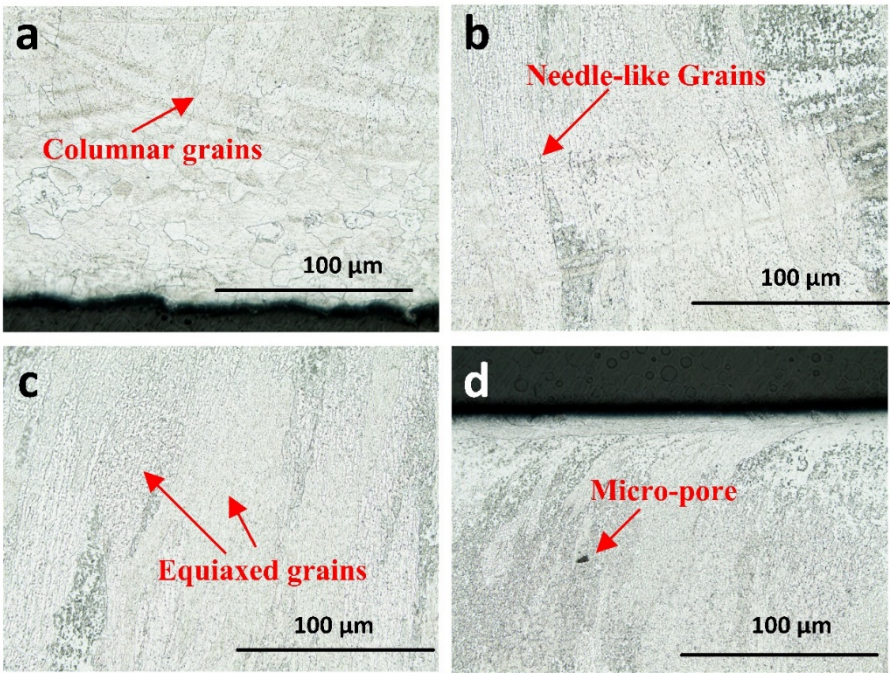

Figure 3 Microstructure of the NiTi WAAM parts cross section: a) magnified microstructure of zone D; b) magnified microstructure of zone E; c) magnified microstructure of zone F; d) magnified microstructure of zone G). Zones D to G are all marked in marked in Fig. 2.

According to EDS analysis, the Ni chemical composition in zone E of Fig. 2c is 51.1 at%. Following the Ni-Ti the equilibrium phase diagram, for a Ni content of 53.5 at%, the expected stable phases below 400 °C are NiTi and Ni_3Ti [38]. Other metastable

178 phases, such as Ni_4Ti_3 and Ni_3Ti_2, can precipitate and decompose to Ni_3Ti after long
179 periods at critical temperatures [34, 37-39]. The non-equilibrium conditions that occur
180 during WAAM prevented the formation of Ni_3Ti precipitates [40, 41].

181 For WAAM, the pre and post-heating caused by subsequent depositions, can
182 drastically impact the as-solidified microstructure and solid-state transformations of the
183 as-built parts. In opposition to welding, where columnar grains are typically prevalent
184 due to the fast cooling, which often lead to a deterioration of mechanical properties in
185 the fusion zone, in the NiTi WAAM parts, these collumnar grains only formed in the
186 first deposited layer. It must be noticed that some micro-pores were observed in the last
187 deposited layer. These are probably formed as a result of entrapped gas during the
188 solidification process or due to some instabilitiy in the sheilding gas flow [42].

189 The microhardness measurements performed in the centreline along the as-built
190 wall (Z direction in Fig.2c) are depicted in Fig.4. The first and second layers exibited
191 lower hardness, from 228 to 236 HV, while the third and subsequent layers kept a
192 relatively constant hardness at 245 HV. The lower hardness in the first deposited layers
193 can be attributed to the different grain morphologies obtained: while for the first layers
194 the existence of collumnar grains decreases the hardness, in the top layers the equiaxed
195 morphology is responsible for an increase in hardness [43,44]. It must be noticed that
196 unlike other materials that exibit a martensitic transformation, such as steels, the
197 cooling rates does not highly impact the resulting hardness.
198

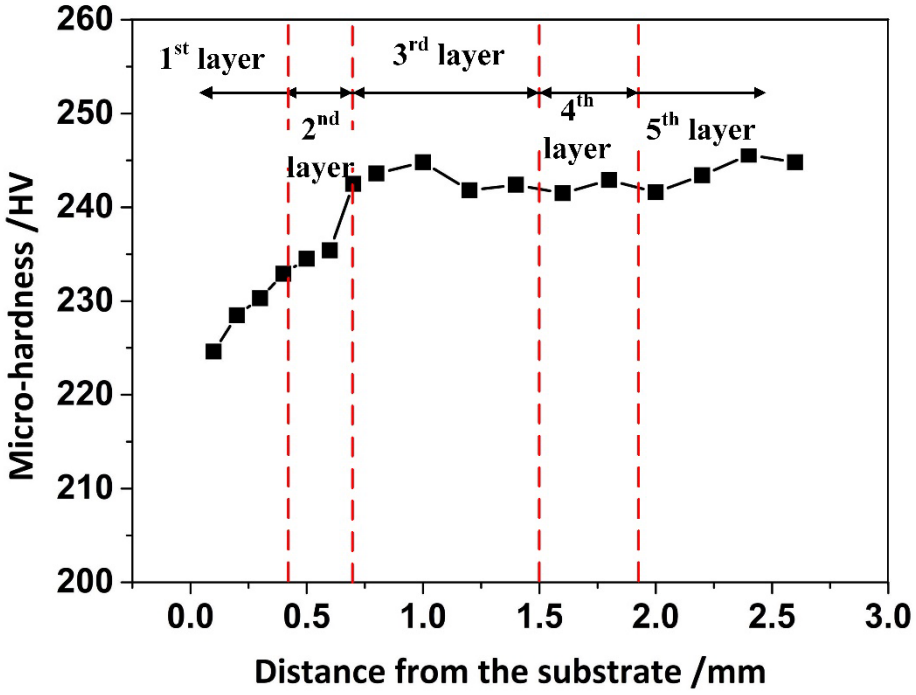

Figure 4 Microhardness along the NiTi WAAM specimen

3.2 Phase transformation characteristics

The phase transformation characteristics of the as-received NiTi wire and as-built WAAM part were analyzed by DSC and the results are depicted in Figure 5. A summary of the transformation temperatures are summarized in Table 1.

Table.1 Transformation temperatures (°C) of the WAAM specimen and as-received NiTi wires.

Materials	A_s	A_f	M_s	M_f
As-received NiTi wire	3.6	16.2	12.5	-2.8
WAAM specimen	-39.2	17.6	-5.4	-43.1

At room temperature, the as-received NiTi wire and WAAM specimen are fully austenitic. The onset temperatures of the as-built part for both M_s and A_f were in the range of -5.4±1.5°C and 17.6±3.2°C, respectively, with a wider transformational range and hysteresis comparing to the as-received NiTi wire, which was measured to be 12.5±2.1°C and 16.2±1.8°C. This change in the transformation temperatures can be related to the differences in grain size and development of residual stresses which are

known to influence the martensitic transformation in NiTi SMAs [45]. Similar results were presented in *ref*. [34], where the transformation temperatures were all below room temperature. The Nickel content increased from 50.5% on as-received wire to 51.1% on deposited layers by EDS. For Ni-rich NiTi, an increase of the Ni matrix content by 1 at. % can drastically reduce the Ms temperature by more than 100 °C [41]. There are multiple factors that can justify the differences in the transformation behavior of the WAAM part compared to the feedstock material. First, the feedstock material, from a microstructural point of view, i.e. grain size, composition and residual stresses, is expected to be homogenous along its length. The same does not occur in the WAAM specimen. As observed before, the grain size changes from the first to the last deposited layer of the as-built part. Differences in grain size have been seen to influence the martensitic transformation for NiTi alloys [46, 47]. For the WAAM part, there is the development of residual stresses which will not be uniform throughout the part height owing to the different thermal cycle conditions. As exemplified in [48], significant differences in the transformation behavior may occur in NiTi processed with localized heat sources, as in WAAM or SLM, as a result of the development of thermally induced residual stresses. In addition, nanoscale precipitation, in this case Ni_4Ti_3, may also change the matrix chemical composition which will modify the transformation temperatures. Previous work on SLM of NiTi in *ref.* [22] reported the formation of nanoscale Ni_4Ti_3. In SLM, the thermal cycle available for Ni_4Ti_3 precipitation is rather small, compared to WAAM. Additionally, during WAAM, as a result of the heat accumulation, it is expected that more favorable conditions for Ni_4Ti_3 precipitation occur as the part is being built. Nonetheless, in WAAM, the time available for precipitation of this phase is within the order of a few seconds, though the volume fraction is expected to be significantly low [49]. Finally, there is the possibility of nano/micro oxidation of Ti during building of the wall. Such oxidation will reduce the available Ti in the matrix also promoting a change in the transformation temperatures [37].

As described above, there are multiple possibilities to explain the differences in the transformation characteristic of the WAAM NiTi parts compared to the as-received

feedstock material. Further research work is in progress to isolate how each one of the aforementioned microstructural features contributed to the change in the transformation temperatures.

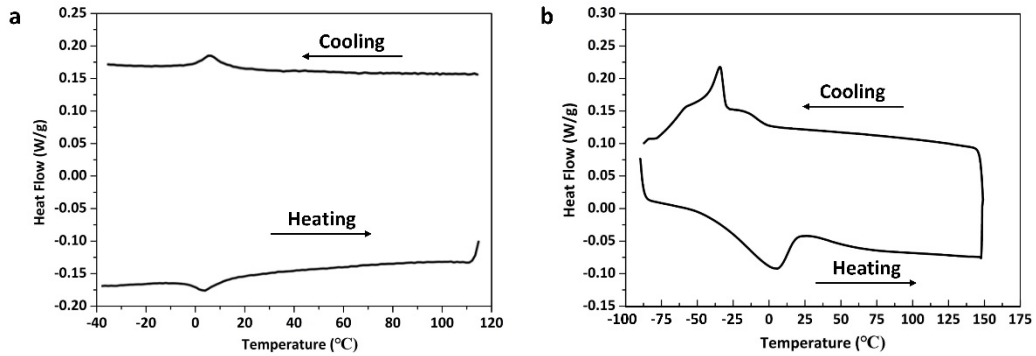

Figure 5 Phase transformation of as-received materials and as-built NiTi WAAM part (a. as-received materials b. as-built NiTi WAAM part)

X-ray diffraction was performed at room temperature to identity the stable phases in the as-built material. The diffractogram depicted in Fig. 7 confirmed that the as-built wall was fully austenitic at room temperature, thus in excellent agreement with the DSC results. From the diffractogram it can be observed the existence of a strong <110> preferred orientation. The existence of a preferred <110> crystallographic orientation in these WAAM NiTi samples can be justified by an abnormal grain growth phenomenon which is caused by a decrease of the surface energy in this specific direction (DOI:10.1115/MSEC2010-34250.

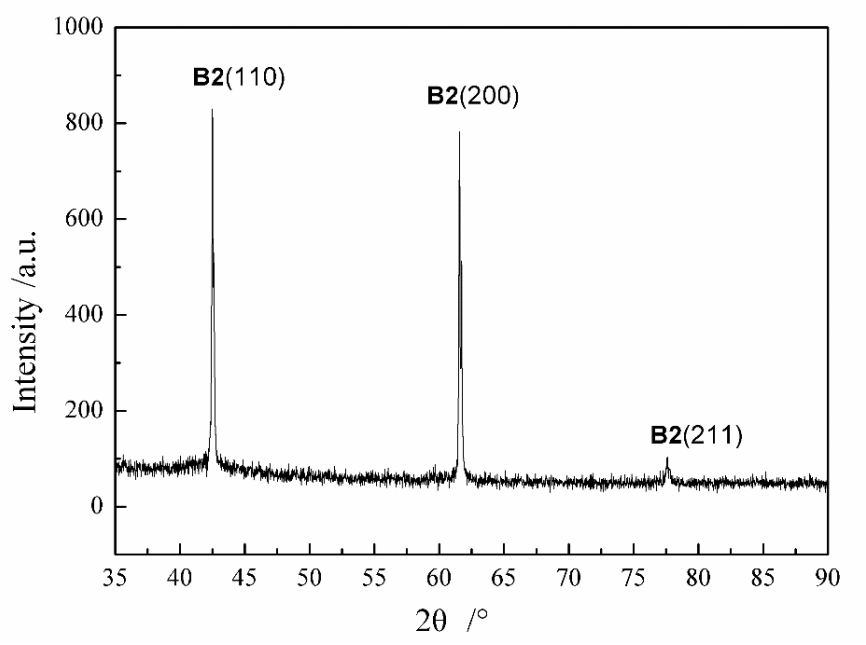

Figure 6 X-ray diffraction pattern of the as-built NiTi WAAM part

3.3 Mechanical properties

To evaluate the mechanical properties of the NiTi WAAM parts conventional tensile testing until fracture was performed. Three samples were analyzed and the typical stress-strain curve of the as-built wall is depicted in Fig. 7. The stress induced transformation from austenite to martensite was seen to occur at 352.8±16.2 MPa and the tensile strenght of the parts was of 571.4±18.6 MPa with a corresponding fracture strain of 16.8±2.4%.

The analysis of Fig. 7 reveals the typical mechanical behaviour of an austenitic NiTi SMA: first, elastic deformation of austenite occurs; then, at around 350 MPa the stress-induced transformation to martensite takes places and proceeds at a near-constant applied stress. At the same time, detwinning of martensite is occurring. The next inflection point, at ≈10% strain, denotes the onset for elastic deformation of detwinned martensite, which eventually started to deform plastically and then frature occurs at ≈17%. The excellent tensile properties are evidenced by these mechanical tests and the existence of small pores in the last deposited layers does not greatly affect the overal performance of the as-built walls.

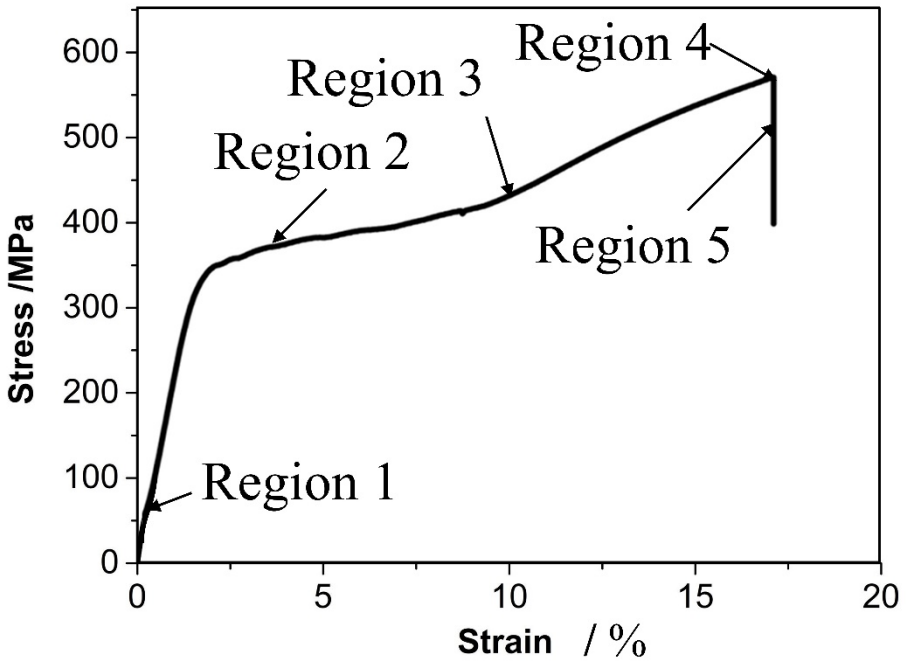

Figure 7 Representative tensile stress-strain curve of a NiTi WAAM specimen

During tensile testing, DIC was used for the analysis of the local mechanical behavior of the specimen at given representative applied stresses. These DIC contours are shown in Fig. 8a to Fig.8e. In region 1 which corresponds to low (≈ 50 MPa) applied external stress no significant strain localization occurrs. When the stress onset for the martensitic transformation (≈ 350 MPa for these NiTi WAAM parts) is reached, the martensite bands start to nucleate as shown in the red box of Fig. 8b, which corresponds to region 2 of Fig. 7. These Lüders/transformation bands are highly mobile and occur at an angle of approximately 55º relative to the load direction in order to fulfill the requirements for macroscopic strain compatibility (least additional elastic deformation) between the undeformed and deformed regions [50, 51].

In region 3, corresponding to the onset for elastic deformation of detwinned martensite, there is reminescent evidence of Lüders bands on the top of the tested specimens (marked with a red rectangle in Fig. 8 c). At this point there is signifcant strain localization at one region of the sample surpassing 9 % strain. This strain concentration may arise from a local microstructural heterogenity, such as a pore, that can act as a stress concentrator. This strain localization is even more noticeable prior to failure (region 4 in Fig.7 and Fig. 8 d) reaching a strain of 17%. At this moment no

evidence of transformation bands exist in the tested sample. The region where strain locallization has occurred is where fracture occurs, which takes places for an external applied stress of ≈570 MPa and a corresponding fracture strain of ≈17%.

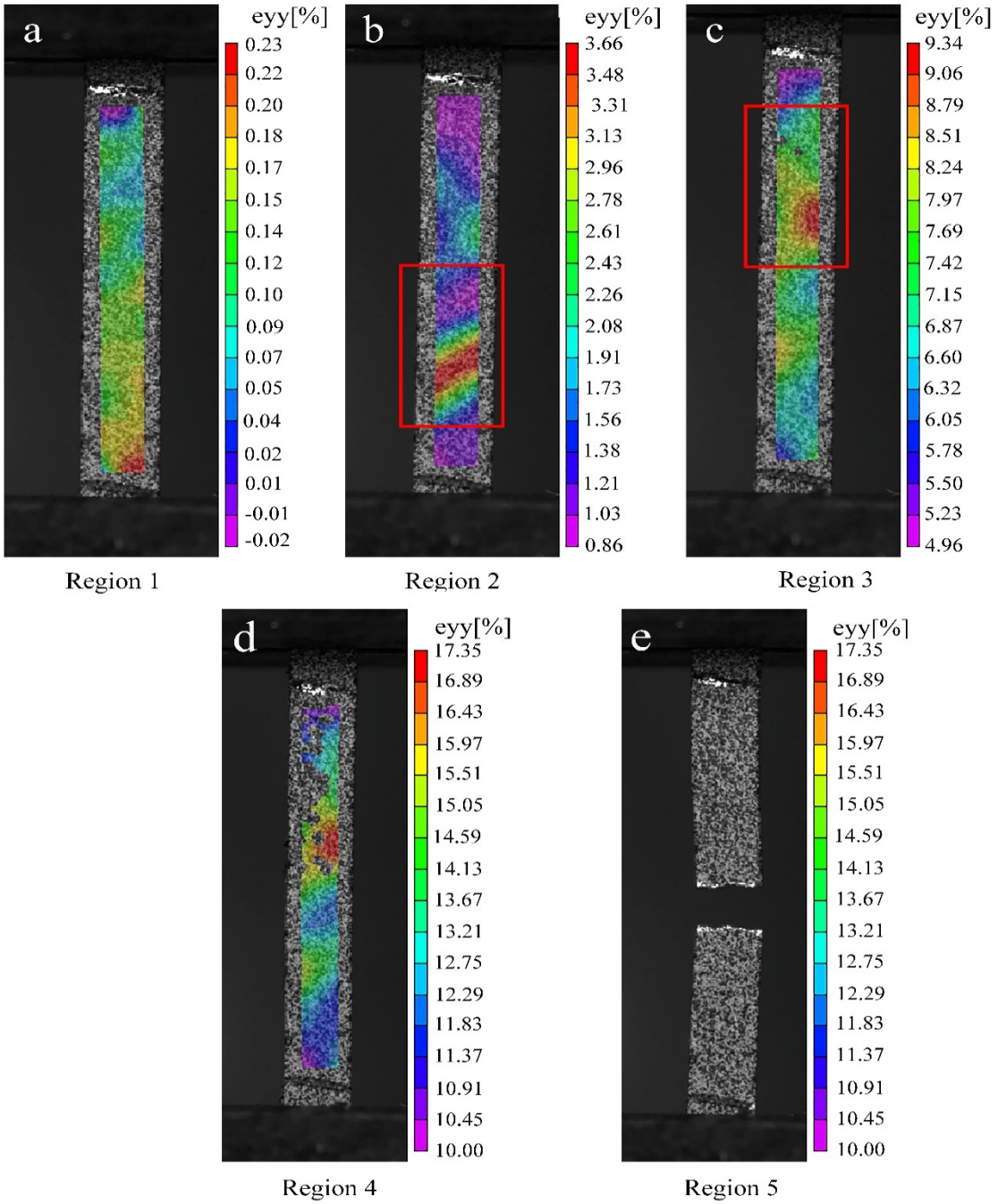

Figure 8 Local mechanical properties of WAAM specimens measured using digital image correlation (a. strain distribution at 50 MPa; b. strain distribution at 350 MPa; c. strain distribution at 420 MPa; d. strain distribution at 550 MPa;e fracture)

SEM imaging of the fracture surfaces was performed after tensile testing (Fig. 9).

A ductile-like fracture surface is clearly observed, as evidenced by the existence of dimples, which is in excellent agreement with the large elongation to fracture of the WAAM NiTi parts. There are no signs of cleavage on the fracture surface. It is noted that nucleation of voids, growth and coalescence are known to start on microcracks or precipitates. Some micro-cracks along the equiaxed grains boundaries can be observed in the high magnification image of Fig. 9b. These cracks can serve as preferential sites for fracture initiation and propagation. The propagation of secondary microcracks occurs as a result of the continuous changes in the local stress state during deformation [52].

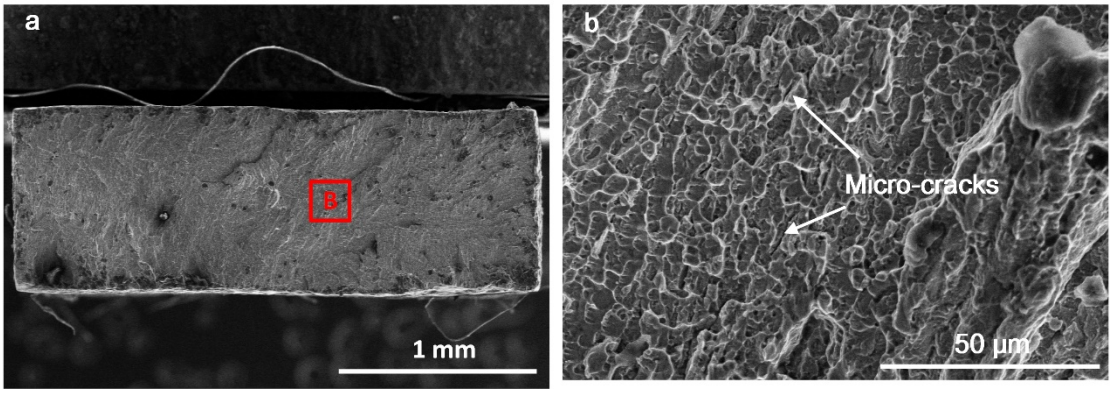

Figure 9 Fracture surface after tensile test (a. macro-structure b. magnified microstructures of zone B in Fig.9a)

Aside from the tensile properties to failure, the cycling behavior of the as-built NiTi parts was also evaluated. The graph in Fig. 10a depicts a total 10 load/unload cycles to a maximum of 6% tensile strain, followed by unloading to a zero-stress condition. It can be seen that the WAAM specimens exhibit good superelastic properties, evidenced by a low irrecoverable strain of 1.13% upon unloading in the first cycle. The plastic strain increased during the first 7 cycles, and reached near a constant value of 2.73% (Fig.8b). For NiTi SMAs, the strain recovery due to the superelastic effect can be as high as 10% [53]. However, there are several aspects that may impair a complete superelastic recovery of the material. These include the testing temperature, the applied strain and strain rate, any thermal and/or mechanical treatment, as well as the grain size of the tested sample [36]. In this investigation, the incomplete recovery of the initial

imposed deformation can arise from the microstructural modifications, i.e. significant differences in grain size induced by the WAAM process [54]. In fact, the existence of a non-homogeneous microstructure, as evidenced by the simultaneous presence of collumnar and equiaxed grains, can promote distintic local mechanical behavior. That is, regions with coarse grain size are expected to be easily deformed when compared to smaller grain sizes and therefore martensite stabilization and subsequent loss of superelasticy can occur [55]. Therefore, the different microstructures, i.e. collumnar at the bottom and equiaxed at the top, along the height of the WAAM part can explain the irrecoverable strain of the as-built part.

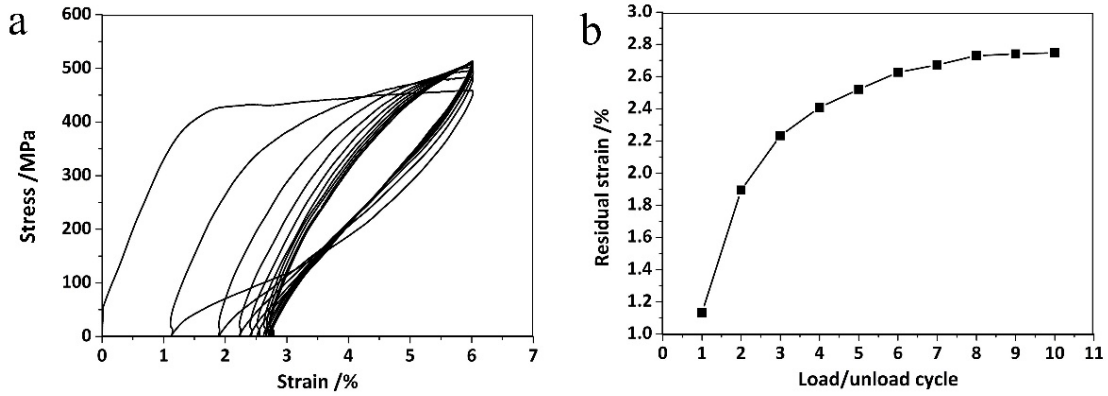

Figure 10 load/unload fuctional fatigue curve of NiTi WAAM specimen (a. load/unload fatigue stress-strain curve, b. accumulated residual strain)

4. Conclusions

Wire and Arc Additive Manufacturing was used to create NiTi shape memory alloy walls, using commercially available Ni-rich NiTi wires as the feedstock material. The following main conclusions can be drawn:

1) A collumnar grain structure was present in the first deposited layers, while towards the top of the wall fine equiaxed grains were formed. This is related to the thermal cycle conditions in both regions.
2) The as-built walls are fully austenitic as confirmed by DSC, XRD and superelastic cycling.

3) The as-built parts exibit superelasticity under tensile conditions and a stable mechanical response is obtained after 7 load/unload cycles.
4) The creation of NiTi parts by WAAM opens new doors for this additive manufacturing technique to be applied for the production of large parts based on these advanced functional materials.

Acknowledgements

This work was supported by Natural Science Foundation of China (No. 51775091, 51405335, 51575383 & 51675031), Science and technology project of Sichuan Province (No. 2018GZ0284), the Natural Science Foundation of Tianjin City (No. 18JCQNJC04100) and the Beijing Municipal Natural Science Foundation (No. 3182020) and the Fundamental Research Funds for the Central Universities (No. YWF-18-BJJ- 244 & YWF-19-BJ-J-232). JPO acknowledges Fundação para a Ciência e Tecnologia (FCT) for its financial support through the project UID/EMS/00667/2019. The authors acknowledge Kaleb Ponder from the Welding Engineering Program at The Ohio State University for the revision of this paper.

References

[1] A. Mitchell, U. Lafont, M. Hołyńska, C. Semprimoschnig. Additive manufacturing -A review of 4D printing and future applications. *Additive Manufacturing*, 2018, 24: 606-626

[2] Jani J M, Leary M, Subic A, Gibson MA. A review of shape memory alloy research, applications and opportunities. *Materials & Design*. 2014, 56: 1078–113.

[3] Gugel H, Schuermann A, Theisen W. Laser welding of NiTi wires. *Materials Science & Engineering A*. 2008, 481-482: 668-671.

[4] Zeng Z, Panton B, Oliveira JP, Han A, Zhou YN. Dissimilar laser welding of NiTi shape memory alloy and copper. *Smart Materials and Structures*. 2015, 24(12): 125036.

[5] Himanshu Sahasrabudhe, Ryan Harrison, Christian Carpenter, Amit Bandyopadhyay. Stainless steel to titanium bimetallic structure using LENS™.

Additive Manufacturing, 2015, 5: 1-8

[6] Dipak Tanaji Waghmare, Chinmaya Kumar Padhee, Ritesh Prasad, Manoj Masanta. NiTi coating on Ti-6Al-4V alloy by TIG cladding process for improvement of wear resistance: Microstructure evolution and mechanical performances. *Journal of Materials Processing Technology*, 2018, 262:551-561.

[7] B. Tam, A. Pequegnat, M. Khan and Y. Zhou, Resistance Microwelding of Ti-55.8 wtpct Ni Nitinol Wires and the Effects of Pseudoelasticity. *Metallurgical and Materials Transactions A*, 2012, 43:2969-2978.

[8] Zhang, Wei, Ao, Sansan, Oliveira, Joao Pedro, Zeng, Zhi, Luo, Zhen, Hao, Zhizhuang. Effect of ultrasonic spot welding on the mechanical behaviour of NiTi shape memory alloys. *Smart Materials and Structures*. 2018 27,085020

[9] Jacob Mingear, Bing Zhang, Darren Hartl, Alaa Elwany, Effect of process parameters and electropolishing on the surface roughness of interior channels in additively manufactured nickel-titanium shape memory alloy actuators. *Additive Manufacturing*, 2019, 27: 565-575

[10]Mohsen Taheri Andani, Soheil Saedi, Ali Sadi Turabi, M. R. Karamooz, Mohammad Elahinia. Mechanical and shape memory properties of porous Ni50.1Ti49.9 alloys manufactured by selective laser melting. *Journal of the Mechanical Behavior of Biomedical Materials*, 2017, 68:224-231.

[11] Bin Zhang, Wenjin Meng, Shuai Shao, Nam Phan, Nima Shamsaei. Effect of Heat Treatments on the Morphology of Pores in Laser Additive Manufactured Parts. *Manufacturing Letters*, https://doi.org/10.1016/j.mfglet.2019.06.005.

[12] K. F. Ayarkwa, S. W. Williams, J. Ding. Assessing the effect of TIG alternating current time cycle on aluminium wire+arc additive manufacture. *Additive Manufacturing,* 2017, 18: 186-193.

[13] Malcolm Dinovitzer, Xiaohu Chen, Jeremy Laliberte, Xiao Huang, Hanspeter Frei. Effect of wire and arc additive manufacturing (WAAM) process parameters on bead geometry and microstructure. *Additive Manufacturing*, 2019, 26: 138-146.

[14] Xiangfang Xu, Jialuo Ding, Supriyo Ganguly, Stewart Williams. Investigation of process factors affecting mechanical properties of INCONEL 718 superalloy in

wire + arc additive manufacture process. *Journal of Materials Processing Technology,* 2019,265:201-209.

[15]Elahinia, M H, Hashemi, M, Tabesh, M, Bhaduri, S B. Manufacturing and processing of NiTi implants: A review. *Progress in Materials Science*. 2012, 57(5): 911-946.

[16] Mohammad Elahinia, Narges Shayesteh Moghaddam, Mohsen Taheri Andani, Amirhesam Amerinatanzi, Reginald F Hamilton. Fabrication of NiTi through additive manufacturing: A review. *Progress in Materials Science*, 2016, 83: 630-663.

[17]Narges Shayesteh Moghaddam,Soheil Saedi,Amirhesam Amerinatanzi, Alejandro Hinojos, Ali Ramazani, Julia Kundin, Michael J. Mills, Haluk Karaca and Mohammad Elahinia. Achieving superelasticity in additively manufactured NiTi in compression without post-process heat treatment. *Scientific Reports*, 2019, 9: 41.

[18]Saedi, S, Turabi, AS, Andani, MT, Haberland, C, Karaca, H, Elahinia, M. The influence of heat treatment on the thermomechanical response of Ni-rich NiTi alloys manufactured by selective laser melting. *Journal of Alloys and Compounds*, 2016, 677:204-210.

[19]Soheil Saedi, Ali Sadi Turabi, Mohsen Taheri Andani, Narges Shayesteh Moghaddam, Mohammad Elahinia and Haluk Ersin Karaca. Texture, aging, and superelasticity of selective laser melting fabricated Ni-rich NiTi alloys. *Materials Science and Engineering: A*,2017,686:1-10.

[20]Reginald F. Hamilton, Beth A. Bimbera, Mohsen Taheri Andani Mohammad Elahinia. Multi-scale shape memory effect recovery in NiTi alloys additive manufactured by selective laser melting and laser directed energy deposition. *Journal of Materials Processing Technology*,2017,250:55-64.

[21] J.P.Oliveira, A.J.Cavaleiro, N.Schell, Andreas Stark, R.M.Miranda, J.L.Ocana, F.M.Braz Fernandes. Effects of laser processing on the transformation characteristics of NiTi: A contribute to additive manufacturing. *Scripta Materialia*,2017,152:122-126

[22] Ji Ma, Brian Franco, Gustavo Tapia, Kubra Karayagiz, Luke Johnson, Jun Liu, Raymundo Arroyave, Ibrahim Karaman and Alaa Elwany. Spatial Control of Functional Response in 4D-Printed Active Metallic Structures. *Scientific Reports*, 2017, 7: 46707.

[23] Tiago A. Rodrigues, V.Duarte,Julian A. Avila,Telmo G. Santos, R.M.Miranda, J.P.Oliveira. Wire and arc additive manufacturing of HSLA steel: Effect of thermal cycles on microstructure and mechanical properties. *Additive Manufacturing*. 2019.27: 440-450.

[24] Derekar, KS. A review of wire arc additive manufacturing and advances in wire arc additive manufacturing of aluminium. *Materials Science and Technology*.2018, 34(8): 895-916.

[25] C.V.Haden, G.Zeng, F.M.Carter III, C.Ruhl, B.A.Krick, D.G.Harlow. Wire and arc additive manufactured steel: Tensile and wear properties. *Additive Manufacturing*. 2017.16: 115-123.

[26] Haibin Geng, Jinglong Li, Jiangtao Xiong, Xin Lin, and Fusheng Zhang. Geometric Limitation and Tensile Properties of Wire and Arc Additive Manufacturing 5A06 Aluminum Alloy Parts. *Journal of Materials Engineering and Performance*. 2017, 26(2): 621-629.

[27] Cong B, Ding J, Williams S. Effect of arc mode in cold metal transfer process on porosity of additively manufactured Al-6.3% Cu alloy. *The International Journal of Advanced Manufacturing Technology*, 2015, 76: 1593–1606.

[28] Qi Z, Cong B, Qi B, Sun H, Zhao G, Ding J. Microstructure and mechanical properties of double-wire + arc additively manufactured Al-Cu-Mg alloys. *Journal of Materials Processing Technology*, 2018, 255: 347–353.

[29] Qi Z, Cong B, Qi B, Zhao G, Ding J. Properties of wire + arc additively manufactured 2024 aluminum alloy with different solution treatment temperature. *Materials Letter*, 2018, 230: 275–278.

[30] Qi Z, Qi B, Cong B, Sun H, Zhao G, Ding J. Microstructure and mechanical properties of wire+ arc additively manufactured 2024 aluminum alloy components: As-deposited and post heat-treated. *Journal of Manufacturing Processes*, 2019, 40:

27-36.

[31] Wang F, Williams S, Colegrove P, Antonysamy A. Microstructure and mechanical properties of wire and arc additive manufactured Ti-6Al-4V. *Metallurgical and Materials Transactions A*, 2013, 44: 968–977.

[32] Martina F, Mehnen J, Williams S, Colegrove P, Wang F. Investigation of the benefits of plasma deposition for the additive layer manufacture of Ti-6Al-4V. *Journal of Materials Processing Technology*, 2012, 212: 1377.

[33] Herzog D, Seyda V, Wycisk E, Emmelmann C. Additive manufacturing of metals. *Acta Materialia*, 2016, 117: 371–392.

[34] Jun Wang, Zengxi Pan, Guangsai Yang, Jian Han, Xizhang Chen, Huijun Li. Location dependence of microstructure, phase transformation temperature and mechanical properties on Ni-rich NiTi alloy fabricated by wire arc additive manufacturing. *Materials Science and Engineering: A*,2019,749:218-222.

[35] M. I. Khan, A. Pequegnat and Y. N. Zhou. Multiple Memory Shape Memory Alloys, *Advanced Engineering Materials*, 2013, 15: 386–393.

[36] J.P.Oliveira, R.M.Miranda, N.Schell, F.M.Braz Fernandes. High strain and long duration cycling behavior of laser welded NiTi sheets. *International Journal of Fatigue*,2016,83(2):195-200.

[37] Oliveira J.P., Barbosa D., Braz Fernandes F. M., Miranda R. M. Tungsten inert gas (TIG) welding of Ni-rich NiTi plates: functional behavior, *Smart Materials and Structures*, 2016, 25(3): 1-7

[38] K. Otsuka, X. Ren, Physical metallurgy of Ti–Ni-based shape memory alloys. *Progress in Matererials Science*. 2005, 50 (5): 511–678.

[39]Dongdong Gu, Chenglong Ma. In-situ formation of Ni_4Ti_3 precipitate and its effect on pseudoelasticity in selective laser melting additive manufactured NiTi-based composites. *Applied Surface Science*. 2018,441: 862-870.

[40] A. Falvo, F. M. Furgiuele and C. Maletta, Laser welding of a NiTi alloy: Mechanical and shape memory behaviour, *Materials Science & Engineering A*, 2005, 412: 235-240.

[41] M. I. Khan, A. Pequegnat and Y. N. Zhou. Multiple Memory Shape Memory Alloys.

499 *Advanced Engineering Materials*, 2013, 15: 386–393.
500 [42] Allen Bagheria, Mohammad J. Mahtabia, Nima Shamsaeib. Fatigue behavior and
501 cyclic deformation of additive manufactured NiTi. *Journal of Materials*
502 *Processing Technology.*. 2018, 252: 440-453.
503 [43] Qi ZW, Qi BJ, Cong BQ, Sun HY, Zhao G, Ding JL. Microstructure and
504 mechanical properties of wire plus arc additively manufactured 2024 aluminum
505 alloy components: As-deposited and post heat-treated. *Journal of Manufacturing*
506 *Process*. 2019, 40: 27-36.
507 [44] Wang LL, Xue JX, Wang Q. Correlation between arc mode, microstructure, and
508 mechanical properties during wire arc additive manufacturing of 316L stainless
509 steel. *Materials Science and Engineering A*. 2019, 751: 183-190.
510 [45] Y. Zheng, F. Jiang, L. Li, H. Yang, and Y. Liu. Effect of ageing treatment on the
511 transformation behaviour of Ti-50.9at.% Ni alloy", *Acta Materialia*, 2008, 56:
512 736-745.
513 [46] Aslan Ahadi, Qingping Sun. Effects of grain size on the rate-dependent
514 thermomechanical responses of nanostructured superelastic NiTi. *Acta Materialia*,
515 2014, 76: 186-197.
516 [47] F. J. Gil, J. M. Manero, J. A. Planell. Effect of grain size on the martensitic
517 transformation in NiTi alloy. *Journal of Materials Science*,1995, 30(10): 2526-
518 2530.
519 [48] J.P. Oliveira, F.M. Braz Fernandes, R.M. Miranda, N. Schell, J.L. Ocaña. Effect of
520 laser welding parameters on the austenite and martensite phase fractions of NiTi.
521 *Materials Characterization*,2016, 119: 148-151.
522 [49] J. P. Oliveira, F. M. Braz Fernandes, R. M. Miranda, N. Schell. On the Mechanisms
523 for Martensite Formation in YAG Laser Welded Austenitic NiTi. *Shape Memory*
524 *and Superelasticity*,2016, 2: 114-120.
525 [50] L. Dong, R. H. Zhou, X. L. Wang, G. K. Hu, Q. P. Sun. On interfacial energy of
526 macroscopic domains in polycrystalline NiTi shape memory alloys. *International*
527 *Journal of Solids and Structures*,2016, 80: 445-455.
528 [51] P. Sedmák, J. Pilch, L. Heller, J. Kopeček, J. Wright, P. Sedlák, M. Frost, P. Šittner.

529 Grain-resolved analysis of localized deformation in nickel-titanium wire under
530 tensile load. *Science*, 2016, 353: 6299.
531 [52] F. Jiang, S. Vecchio Kenneth. Fracture of Nitinol under quasistatic and dynamic
532 loading. *Metallurgical and Materials Transactions A*, 2007, 38: 2907-2915.
533 [53] Yao Xiao, Pan Zeng, Liping Lei, Yanzhi Zhang. In situ observation on temperature
534 dependence of martensitic transformation and plastic deformation in
535 superelastic NiTi shape memory alloy. *Materials & Design*, 2017, 134:111-120.
536 [54] Zeng Z, Oliveira JP, Yang M, Song D, Peng B. Functional fatigue behavior of NiTi-
537 Cu dissimilar laser welds. *Materials & Design*. 2017, 114(15): 282-287.
538 [55] J. P. Oliveira, F. M. Braz Fernandesa, N. Schell, R. M. Miranda. Martensite
539 stabilization during superelastic cycling of laser welded NiTi plates. *Materials*
540 *Letters*, 2016, 171: 273-276.
541